A Convex-Hull based Method with Manifold Projections for Detecting Cell Protrusions

Zhaoke Huang[a,*], Zihan Wu[a], Hong Yan[a]

[a]*Department of Electrical Engineering, City University of Hong Kong, Hong Kong 999077, China*

Abstract

Cell protrusions play an important role in a variety of cell physiological processes. In this paper, we propose a convex-hull based method, combined with manifold projections, to detect cell protrusions. A convex hull is generated based on the cell surface. We consider the cell surface and the convex hull as two manifolds, which are diffeomorphic, and define a depth function based on the distance between the cell surface and the convex hull. The extreme points of the depth function represent the positions of cell protrusions. To find the extreme points easily, we project the points on the cell surface onto the convex hull and expand them in spherical polar coordinates. The extreme points are found by computing the derivative of the depth function. Experiments on three datasets show that the proposed method has a robust performance.

Keywords: Convex hull, Manifold Projections, Detecting cell protrusions

1. Introduction

Cell protrusions are plasma membrane structures based on actin molecules that protrude from the edge of a cell. They play an important role in a variety of cell physiological processes, such as cell migration, maintenance of cell morphology, cell-cell signal communication, remodeling the cytoskeleton, and neuronal growth cone formation and development [1, 2]. Each protrusion has a specific function and exhibits different shapes. Cell protrusions are broadly

*Corresponding author

Email address: z.huang@cityu.edu.hk (Zhaoke Huang)

classified according to their shape and function, mainly lamellipodia, membrane blebs, and filopodia [3, 4]. To understand the biological significance of various cell protrusions, it is essential to understand their shape changes. However, due to technical difficulties, detecting cell protrusions remains difficult as they are difficult to observe, especially in vivo, because of their small size, lack of specific labeling, and often unstable nature. Therefore, the detection of cell protrusions requires study.

With the development of live-cell imaging technology, the behavior of cells can be visualized with extraordinary precision and detail. Methods and tools to detect cell protrusions [5, 6] have limitations. Some, like FiloDetect [7], CellGeo [8], and ADAPT [9], were developed for 2D cell images. Although they could be extended to 3D cell image analysis, straightforward extensions are unlikely to be effective. Some cell protrusion detection methods were developed for a particular kind of protrusion. FiloDetect [7], Filopodyan [10], and FiloQuant [5] were designed to analyze filopodia, not lamellipodia or membrane blebs. Limitations of these methods include a lack of customizable options, being developed on simple samples, and a lack of mathematical analysis. U-shape3D [6] advanced cell protrusion detection methods by using supervised learning to detect cell protrusions, but needs a lot of labeled protrusion data, which is difficult to obtain manually, to train the model.

In this work, we propose a convex-hull based method, combined with manifold projections, to detect cell protrusions. The main idea of our method is to detect cell protrusions based on their geometry. Intuitively, the geometry of cell protrusions resembles a mountain. If we find the extreme point (the peak), we should find the cell protrusion. So, we want to construct a geometric invariant function, which should be a distance function, to represent the shape of cell protrusions. One option is to set a reference point (such as the center of mass) inside the cell and calculate the distance from all points on the cell surface to the reference point as a distance function. Expanding the projection of the points in spherical polar coordinates would lead to multiple overlapping points occurring, causing the function to become multivalued after the projection. Thus, in this study, a convex hull is used as an intermediate step to avoid this problem. The core of the method is to define a distance function based on the convex hull of the cell surface and find the extreme points of this function to identify cell protrusions. This method can detect different types of cell protrusions using unsupervised learning.

The proposed method is briefly summarized as follows. Initially, generate a convex hull based on the cell surface. Consider the cell surface and the

convex hull as two manifolds, which are diffeomorphic. Then, calculate the distances from a point on the cell surface to all faces of the convex hull, where the minimum distance is defined as the depth of the point. This defines a depth function on the cell surface. Since finding the extreme points of the depth function on the cell surface manifold is complicated, the points on the cell surface are projected onto the convex hull and expanded into spherical polar coordinates. Finally, the extreme points are found by computing the derivative of the depth function.

Our main contributions can be summarized as:

- We propose a convex-hull based method combined with manifold projections to detect cell protrusions. Meanwhile, we mathematically prove the feasibility of the proposed method.
- We create a convenient coordinate system based on the convex hull of the cell surface, which can provide a reference frame for quantifying the geometry of cell protrusions.
- We define a depth function based on the distance between the cell surface and its convex hull, which can provide important information to identify the shape of cell protrusions.
- We consider the cell surface and the convex hull as two manifolds, which are diffeomorphic. To easily find the positions of cell protrusions, the points on the cell surface are projected onto the convex hull and expanded in spherical polar coordinates.

2. Related Work

At present, most methods proposed to detect cell protrusions were developed for filopodia. Well-known methods are: FiloDetect [7], the first automated tool for detecting, counting, and measuring the length of filopodia in fluorescence microscopy images. It employs intensity-based thresholding and a combination of morphological operations to detect filopodia. CellGeo [8], a computational platform to allow simultaneous, automated tracking and analysis of dynamic changes in cell shape, including protrusions ranging from filopodia to lamellipodia. It uses the medial axis transform to represent any arbitrary cell shape to identify cell protrusions. Filopodyan [10], an open-source pipeline for the analysis of filopodia. It generates a descriptive

dataset of filopodial properties to describe filopodial shape, dynamics and fluorescence. Then it detects filopodia using cross-correlation analysis and hierarchical clustering. FiloQuant [5], a freely available ImageJ plugin to detect filopodia-like protrusions in both fixed- and live-cell microscopy data. All have shortcomings. (1) CellGeo and FiloQuant only work on 2D images and do not yet support 3D analyses. (2) FiloDetect and Filopodyan will not work well on noisy images. (3) FiloDetect, Filopodyan, and FiloQuant are limited to the detection of filopodia and other finger-like protrusions. A robust and automated detection method, u-shape3D, was proposed for subcellular morphological motifs in 3D microscopy images [6]. It decomposes the cell surface into convex patches and classifies each patch by a trained SVM, using supervised learning to detect cell protrusions, but manually labeling each patch is very difficult. Several other works have investigated cell protrusions [11, 12, 13, 14, 15]. However, there is still a lack of effective methods to detect cell protrusions based on geometric analysis.

3. Method

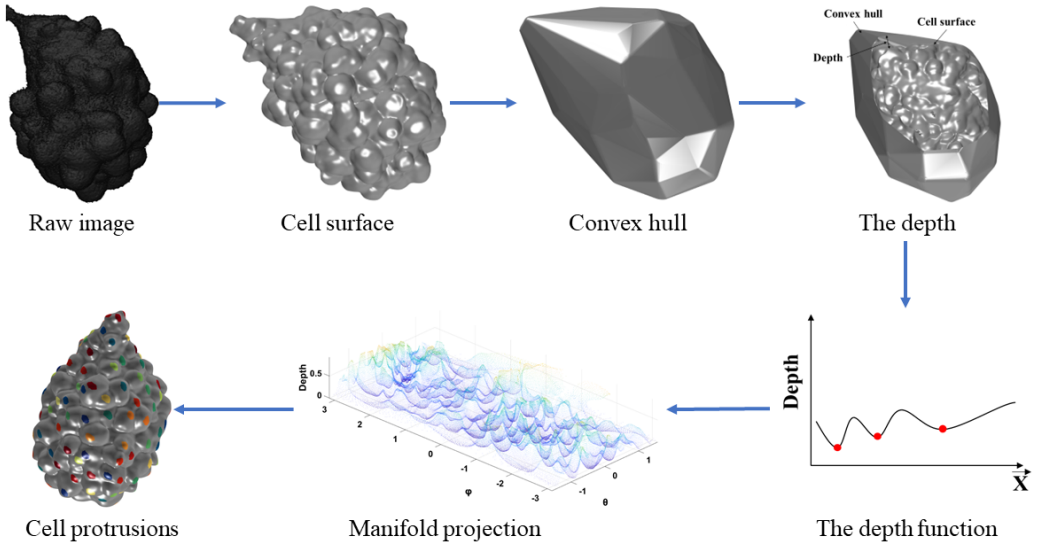

Figure 1: The framework of the proposed method.

We propose a convex-hull based method combined with manifold projections to detect cell protrusions. The framework of this method is shown in

Figure 1. First, the quickhull algorithm [16] generates a convex hull based on the cell surface. Next, a depth function is defined based on the distance between the cell surface and its convex hull. To easily find the positions of cell protrusions, the points on the cell surface are projected onto the convex hull and expanded in spherical polar coordinates. Finally, the derivative of the depth function is computed to find the cell protrusions.

In what follows, the definitions of manifolds relevant to this work are reviewed and the method to detect cell protrusions is introduced.

3.1. Mathematical background

As the cell surface and the convex hull are considered as two smooth manifolds M and N in this study, smooth functions on manifolds and smooth maps between manifolds are introduced.

Definition 1. *Let $f : M \to \mathbb{R}$ be a continuous function defined on the smooth manifold M. If for a point $p \in M$, there exists a smooth chart (U, φ) for M such that $p \in U$ and $f \circ \varphi^{-1} : \varphi(U) \to \mathbb{R}$ is a smooth function at the point $\varphi(p)$, f is smooth at the point p. If f is smooth at every point of M, f is a smooth function on the M.*

The set of all smooth functions on the M is denoted as $C^\infty(M)$. Because sums and constant multiples of smooth functions are smooth, $C^\infty(M)$ is a vector space over $\mathbb{R}$. The definition of smooth functions generalizes easily to maps between manifolds.

Definition 2. *Let M, N be smooth manifolds, and let $F : M \to N$ be a continuous map. If for a point $p \in M$, there exist smooth charts (U, φ) for M and (V, ψ) for N such that $p \in U$, $F(p) \in V$, and $\psi \circ F \circ \varphi^{-1} : \varphi(U \cap F^{-1}(V)) \to \psi(V)$ is a smooth function at the point $\varphi(p)$, F is smooth at the point p. If F is smooth at every point of M, F is a smooth function from M to N.*

Definition 3. *Suppose M and N are smooth manifolds and $f : M \to N$ is a homeomorphism. If $f : M \to N$ and its inverse map $f^{-1} : N \to M$ are smooth maps, we say that $f : M \to N$ is a diffeomorphism.*

In the following subsections, the depth function and projection map between manifolds based on these definitions are constructed.

3.2. Convex hull

The convex hull is a basic concept in computational geometry. Because the convex hull has a relatively stable geometric pattern, it is widely used in pattern recognition [17], image registration [18], and shape detection [19, 20]. The convex hull of a shape is the smallest convex set that contains it. In this work, the convex hull is used to mediate the detection of cell protrusions. The convex hull provides two important pieces of information for further analysis: a minimal convex polyhedron enclosing the entire cell surface; and a new coordinate system for the points of the cell surface.

3.3. Depth function

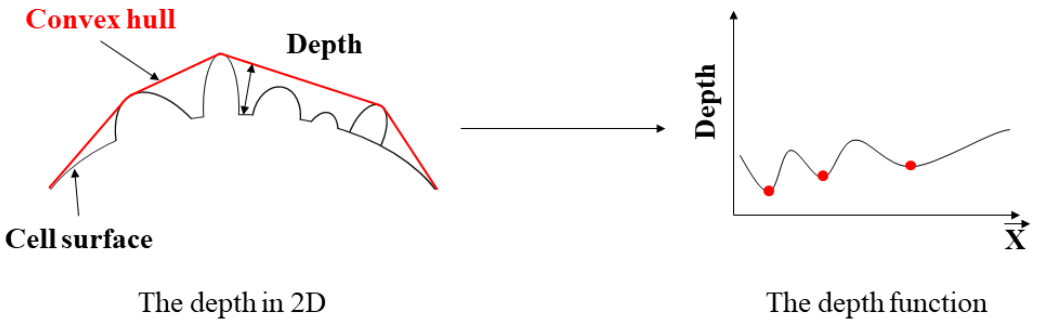

Figure 2: The depth function on the cell surface.

After generating the convex hull, a depth function is defined based on the distance between the cell surface and its convex hull. The depth function is represented by $h : M \to \mathbb{R}^*$. According to Definition 1, it is a smooth function. The detailed steps to obtain the depths of all points are: Calculate the distance from the point p_i on the cell surface to the jth face of the convex hull, denoted by $\mathbf{Dist}_{ij}$. For each point p_i on the cell surface, the minimum distance in $\mathbf{Dist}_i$ is defined as the depth of the point p_i, denoted by $\mathbf{D}_i$. Iterate over all the points on the cell surface and get all the depths. Figure 2 describes the depth function on the cell surface. For ease of description, the cell surface and the convex hull are shown in 2D. The black line represents the cell surface and the red line represents the convex hull. The center of the cell protrusion is closer to the convex hull than the points near it. So, in the depth function graph, the local minima are the positions of cell protrusions (the red dots).

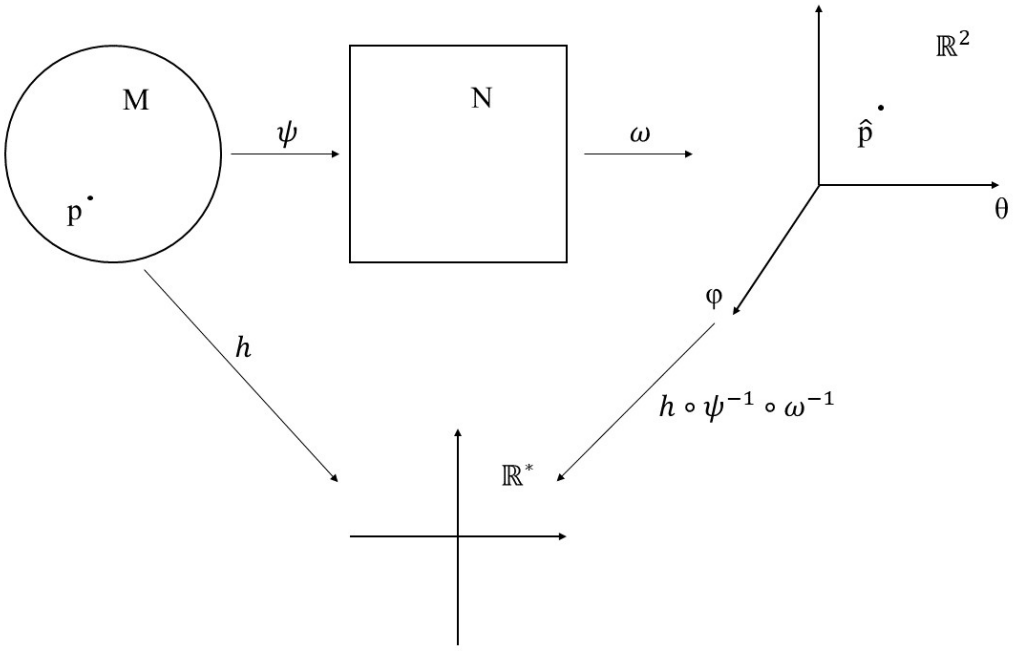

Figure 3: The projection process.

3.4. Projection map

To find the local minima in the depth function, a regular way is to take the derivative of the depth function. The cell surface M is a smooth manifold, and let (U, φ) be a smooth coordinate chart on M. Solve the following equation:

$$\left.\frac{\partial}{\partial x^i}\right|_p h = \left.\frac{\partial}{\partial x^i}\right|_{\varphi(p)} (h \circ \varphi^{-1}) = 0, \tag{1}$$

where $\partial/\partial x^i|p$ is the derivation that takes the ith partial derivative of h at p. However, there are several difficulties in solving this equation. A good φ is not known and two eigen-bases of the tangent space need to be found. However, φ and the eigen-bases vary for each point on the cell surface, which creates a computationally intensive problem.

To handle these difficulties, the points on the cell surface are projected onto the convex hull and expanded in spherical polar coordinates. The process is described in Figure 3. According to Definition 3, the cell surface M and the convex hull N are diffeomorphic. Hence, two projection maps $\psi : M \to N$ and $\omega : N \to \mathbb{R}^2$ can be defined. The map ψ is equivalent

to projecting the points on M onto N. According to Definition 2, the map ψ is a smooth map. The map ω is equivalent to expanding the points on N in spherical polar coordinates. So, the new projection depth function is $\hat{h} = h \circ \psi^{-1} \circ \omega^{-1} : \mathbb{R}^2 \to \mathbb{R}^*$. Originally, we wanted to find the set of points $p \in M$ such that $\mathrm{d}h_p = 0$. Now, the problem is converted to find the set of points $\hat{p} \in S$, where S represents the projection space, such that $\mathrm{d}\hat{h}_{\hat{p}} = 0$, which satisfies the following equivalent relation:

$$\mathrm{d}h_p = 0 \Longleftrightarrow \mathrm{d}\hat{h}_{\hat{p}} = 0. \tag{2}$$

To prove the above relation, we only have to prove theorem 1.

Theorem 1. *Let M, N be smooth manifolds, and $F : M \to N$ be a diffeomorphism. Let $h : N \to \mathbb{R}$ be a smooth function. If $P \subseteq N$ is the critical point set of h and $Q \subseteq M$ is the critical point set of $H = h \circ F$, then $F^{-1}(P) = Q$.*

To prove Theorem 1, define the induced function $H = h \circ F$ to manipulate h on M. It is natural to consider the $F^*(\mathrm{d}h) : TM \to \mathbb{R}$ on M, where T represents the tangent bundle space, as corresponding to $\mathrm{d}h$ on N:

$$F_p^*(\mathrm{d}h)(v) = \mathrm{d}h_{F(p)}\left(dF_p(v)\right), \quad v \in T_pM. \tag{3}$$

We can calculate $F^*(\mathrm{d}h)$ based on Lemma 2.

Lemma 2. *Let M, N be smooth manifolds and $F : M \to N$ be a diffeomorphism. Let $h : N \to \mathbb{R}$ be a smooth function. Denote $H = h \circ F$. We have*

$$F^*(\mathrm{d}h) = \mathrm{d}H. \tag{4}$$

Proof of Lemma 2. $\forall p \in M, v \in T_pM$, we have

$$\begin{aligned}
\left(F^*\mathrm{d}h\right)_p(v) &= \left(\mathrm{d}F_p^*\left(\mathrm{d}h_{F(p)}\right)\right)(v) \\
&= \mathrm{d}h_{F(p)}\left(\mathrm{d}F_p(v)\right) \\
&= \mathrm{d}F_p(v)h \\
&= v(h \circ F) \\
&= \mathrm{d}(h \circ F)_p(v).
\end{aligned}$$

□

Now, Lemma 2 is used to prove Theorem 1.

Proof of Theorem 1. It suffices to show that $F^{-1}(P) \subseteq Q$ and $Q \subseteq F^{-1}(P)$.

1) $Q \subseteq F^{-1}(P)$:
Consider $q \in Q$ and $v \in T_{F(q)}N$. We have

$$\mathrm{d}H_q = 0.$$

Since F is a diffeomorphism, we have $\mathrm{d}F_q^{-1}(v) \in T_qM$. By the pull back F^*, we have

$$\mathrm{d}h_{F(q)}(v) = [F_q^*(\mathrm{d}h)](\mathrm{d}F_q^{-1}(v)). \tag{5}$$

From Lemma 2, noticing $\mathrm{d}H_q = 0$, we have

$$[F_q^*(\mathrm{d}h)](\mathrm{d}F_q^{-1}(v)) = \mathrm{d}H_q(\mathrm{d}F_q^{-1}(v)) = 0. \tag{6}$$

Thus,

$$\mathrm{d}h_{F(q)}(v) = 0, \quad \forall v \in T_{F(q)}N. \tag{7}$$

which is exactly

$$\begin{aligned} & F(q) \in P && (8)\\ \Rightarrow \quad & q \in F^{-1}(P) && (9)\\ \Rightarrow \quad & Q \subseteq F^{-1}(P). && (10) \end{aligned}$$

2) $F^{-1}(P) \subseteq Q$:
For all $p \in P$,

$$\mathrm{d}h_p = 0. \tag{11}$$

Similar to the proof of 1), $\forall v \in T_{F^{-1}(p)}M$, we have

$$\mathrm{d}H_{F^{-1}(p)}(v) = \mathrm{d}h_p(\mathrm{d}F_{F^{-1}(p)}(v)) = 0. \tag{12}$$

Thus,

$$F^{-1}(p) \in Q, \tag{13}$$

which gives

$$F^{-1}(P) \subseteq Q. \tag{14}$$

□

Hence, from Theorem 1, calculate the critical point set of $\hat{h}$ to get the critical point set of h.

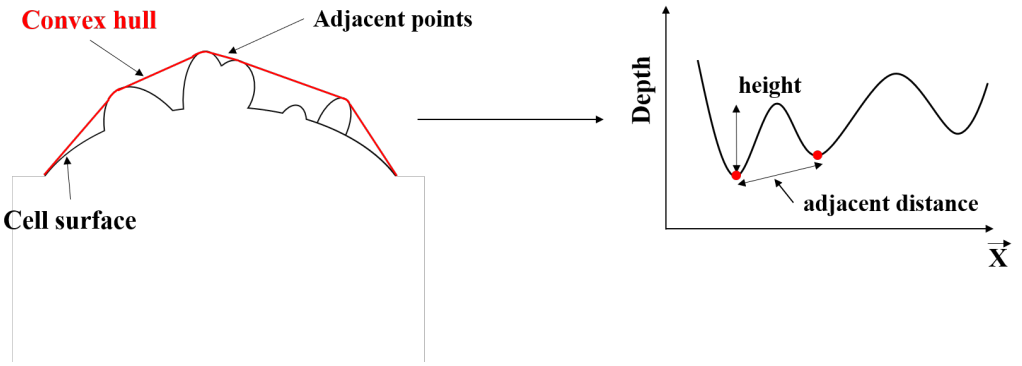

Figure 4: The definition of two parameters.

3.5. Identifying cell protrusions

The positions of the cell protrusions were obtained in the previous subsection. To obtain complete cell protrusions, two parameters were designed for our method. Figure 4 shows the definition of the two parameters. One is the adjacent distance α. If the distance between two adjacent local minima is less than α, then merge the two points as some adjacent local minima may be on the same protrusions (like Figure 4). The other is the height β, such that a cell protrusion is obtained if its trough is more than β. If the areas of two cell protrusions overlap, they are merged. The two rules calibrate the proposed method to reduce the number of misleading or incorrect local minima on cell protrusions. All cell protrusions are obtained by searching all the troughs where local minima are located.

3.6. Implementation

Algorithm 1 Cell Protrusion Detection Algorithm

1: BuildConvexHull()
2: ComputePlaneEquations()
3: CalculateDistances()
4: FindMinimumDistances()
5: CalculateProjections()
6: Convert2SphericalCoordinates()
7: FindMinimumDepths()
8: ExtractCellProtrusions()

The method is summarized in Algorithm 1. The function BuildConvexHull() in line 1 generates the convex hull based on the cell surface. The function ComputePlaneEquations() in line 2 computes plane equations for all faces of the convex hull. The function CalculateDistances() in line 3 calculates the distance from point i on the cell surface to face j of the convex hull, denoted by $\mathbf{Dist}_{ij}$. The function FindMinimumDistances() in line 4 finds the minimum distance in $\mathbf{Dist}_i$. The function CalculateProjections() in line 5 projects all points on the cell surface onto the convex hull. The function Convert2SphericalCoordinates() in line 6 expands all points in spherical polar coordinates. The function FindMinimumDepths() in line 7 finds the local minima in the projection depth function. The function ExtractCellProtrusions() in line 8 extracts the shape of cell protrusions according to the two parameters α and β.

4. Experiments

To validate the proposed method, three types of cell protrusions were used in experiments. They were blebs on MV3 melanoma cells, filopodia on human bronchial epithelial cells (HBECs), and lamellipodia on dendritic cells. We evaluated the proposed method in two ways. First, the number of cell protrusions was used as an index to test the proposed method. The number of manually determined cell protrusions was used as a benchmark. Second, to quantitatively evaluate the detection performance of the proposed method, we compared the positions of the detected cell protrusions against those of the manually determined cell protrusions. Finally, we also compared the proposed method with the existing methods. For each of the images, three experienced researchers visually inspected the protrusions of each cell and identified the locations of each cell protrusion. These data were used to give the number and positions of cell protrusions present for each cell.

4.1. Datasets

The details of the three types of cells are described as follows. Fig. 5 shows examples of these three types of cell protrusions.

- **MV3 melanoma cells**. The dataset has 19 cell images of $512 \times 512 \times 151$ pixels. The number of cell protrusions counted from these cells ranged from around 150 to around 240.

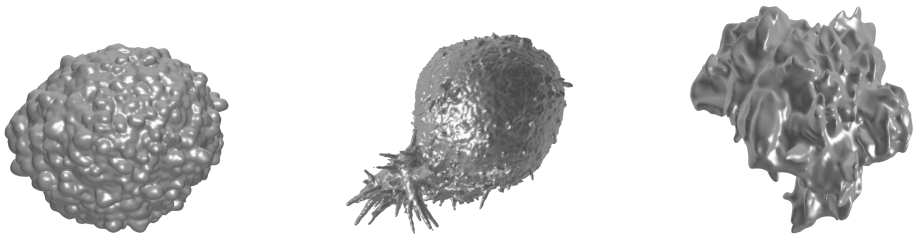

(a) blebs (b) filopodia (c) lamellipodia

Figure 5: Examples of three types of cell protrusions.

- **Human bronchial epithelial cells**. The dataset has 14 cell images of $512 \times 512 \times 501$ pixels. The number of cell protrusions counted from these cells ranged from around 40 to around 90.

- **Dendritic cells**. The dataset has 13 cell images of $512 \times 512 \times 201$ pixels. The number of cell protrusions counted from these cells ranged from around 80 to around 120.

4.2. Evaluation of the number of cell protrusions

First, we use the number of cell protrusions as an index to test the proposed method. Figs. 6, 7 and 8 show the results of the comparison of the proposed method and the manual counting method for the three types of cells. The number of cell protrusions that the proposed method outputs closely matches the median cell protrusion number from the manually labeled data. For the 19 MV3 melanoma cells, 14 HBECs, and 13 dendritic cells, the percent errors of the proposed method ranged from 0.43% to 3.07%, 2.33% to 7.27% and 3.61% to 7.69%, respectively. The performance of the proposed method is better at detecting blebs than filopodia and lamellipodia as their features and shapes are more complex than those of blebs. Although the manual counting results from the individuals were different, they varied within a small range and the results from the proposed method were close to them. Another finding was that the number of cell protrusions obtained by the proposed method was slightly less than that of the manual counting method on the HBECs and dendritic cells. Filopodia and lamellipodia were nested with smaller filopodia and lamellipodia, which caused the proposed method to not be able to find the small protrusions.

Then we also compared the proposed method with the existing methods Chan-Vese model (CVS) [21], convolutional neural network (CNN) [11],

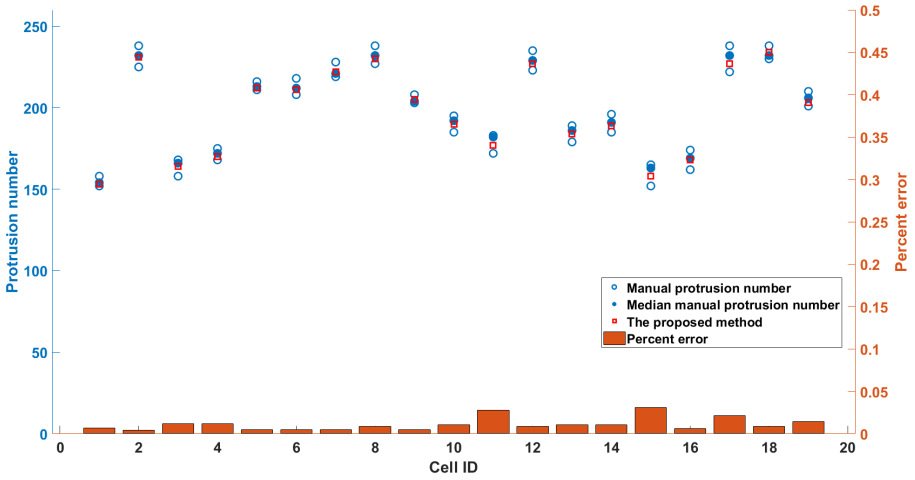

Figure 6: Comparison of the proposed method and the manual counting method in MV3 melanoma cells.

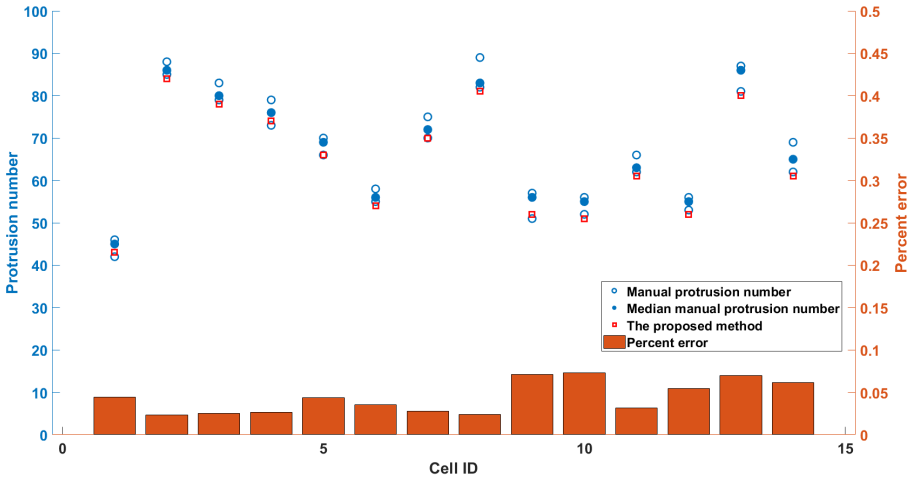

Figure 7: Comparison of the proposed method and the manual counting method in HBECs.

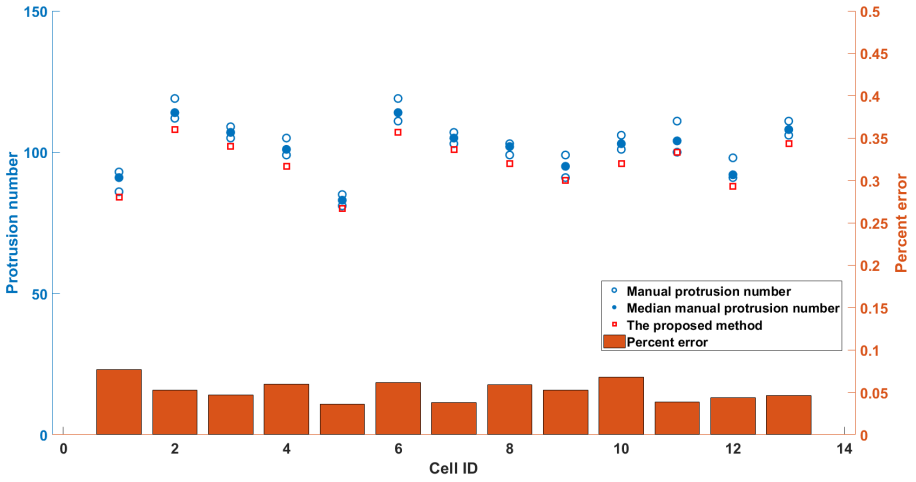

Figure 8: Comparison of the proposed method and the manual counting method in dendritic cells.

and support vector machine (SVM) [6]. Table 1 shows the average accuracy between the proposed method and existing methods on the three types of cells on number detection. In all three datasets, the proposed method outperformed the other methods. The same phenomenon is that all methods performed better at detecting blebs than filopodia and lamellipodia.

Metric	Method	MV3 melanoma cells	HBECs	Dendritic cells
Number	CVS	0.806 ± 0.039	0.759 ± 0.066	0.721 ± 0.068
	CNN	0.925 ± 0.021	0.903 ± 0.025	0.841 ± 0.035
	SVM	0.973 ± 0.013	0.938 ± 0.021	0.882 ± 0.024
	our method	0.989 ± 0.008	0.956 ± 0.012	0.947 ± 0.013

Table 1: Comparison between the proposed method and existing methods on the three types of cells.

4.3. Evaluation of the positions of cell protrusions

Second, to quantitatively evaluate the performance of the proposed method for cell protrusion location, we compared the positions of the detected cell protrusions against those of the manually determined cell protrusions. According to the majority rule, the ground truth for the positions of the cell

protrusions was taken as the combination of the manually annotated positions by the three researchers. We also conducted a parametric analysis. Table 2 shows the average accuracy the proposed method outputs under different parameter values. The values in parentheses represent α and β, respectively. From Table 1, it can be found that the height of lamellipodia is higher than that of the other two cell protrusions and blebs are more densely distributed than the other two cell protrusions. The average accuracy of position detection of the three types of protrusions is above 93%.

Parm	MV3 melanoma cells	Parm	HBECs	Parm	Dendritic cells
(3,2)	0.959 ± 0.010	(4,5)	0.948 ± 0.013	(5,6)	0.938 ± 0.015
(4,2)	0.973 ± 0.009	(5,5)	0.948 ± 0.013	(6,6)	0.938 ± 0.015
(5,2)	0.973 ± 0.009	(6,5)	0.929 ± 0.016	(7,6)	0.921 ± 0.016
(3,3)	0.948 ± 0.011	(4,6)	0.936 ± 0.014	(5,7)	0.918 ± 0.019
(4,3)	0.956 ± 0.010	(5,6)	0.936 ± 0.014	(6,7)	0.918 ± 0.019
(5,3)	0.956 ± 0.010	(6,6)	0.921 ± 0.017	(7,7)	0.901 ± 0.020

Table 2: The average accuracy the proposed method outputs under different parameter values.

Then we also compared the proposed method with the above existing methods. Table 3 shows the average accuracy between the proposed method and existing methods on the three types of cells on position detection. In all three datasets, the proposed method outperformed the other methods. This indicates that the proposed method has a good performance.

Metric	Method	MV3 melanoma cells	HBECs	Dendritic cells
Position	CVS	0.785 ± 0.068	0.706 ± 0.084	0.716 ± 0.076
	CNN	0.914 ± 0.021	0.866 ± 0.032	0.809 ± 0.026
	SVM	0.962 ± 0.013	0.929 ± 0.021	0.869 ± 0.023
	our method	0.973 ± 0.009	0.948 ± 0.013	0.938 ± 0.015

Table 3: Comparison between the proposed method and existing methods on the three types of cells.

5. Conclusion

We proposed a convex-hull based method combined with manifold projections to detect cell protrusions. It introduces three advantages. First, the

convex hull based on the cell surface is introduced as a convenient coordinate system, which can provide a reference frame to quantify the geometry of cell protrusions. Second, a depth function based on the distance between the cell surface and its convex hull was defined. This can provide important information to identify the shape of cell protrusions. Third, the cell surface and the convex hull are considered as two diffeomorphic manifolds. The positions of cell protrusions are easily found by projecting the points on the cell surface onto the convex hull and expanding them in spherical polar coordinates. Experiments on three types of cells showed that the proposed method performed well and provides fresh insight into ways to detect cell protrusions.

The greatest limitation of the proposed method is that it needs segmented single-cell images. If the segmented image is not accurate, the effectiveness of the method will be greatly reduced. Currently, there are two types of cell segmentation methods: (1) manual cell segmentation and (2) automated cell segmentation. However, the manual cell segmentation method is reliable but time-consuming. The automated cell segmentation method is not infallible to extract the cell surface. We think the proposed method integrated with the automated cell segmentation method coupled with manual correction has the potential to be a more robust cell protrusion analysis pipeline. In addition, the performance of this method in detecting complex cell protrusions should be improved, especially the cell protrusions with folds. The main reason is that a big cell protrusion has many extreme points in the depth function. More parameters and strategies need to be designed to handle this limitation.

Acknowledgement

This work is supported by Hong Kong Innovation and Technology Commission (InnoHK Project CIMDA), Hong Kong Research Grants Council (Project 11204821), and City University of Hong Kong (Projects 9610034 and 9610460).

References

[1] P. K. Mattila, P. Lappalainen, Filopodia: molecular architecture and cellular functions, Nature Reviews Molecular Cell Biology 9 (6) (2008) 446–454. doi:10.1038/nrm2406.
URL https://doi.org/10.1038/nrm2406

[2] K. Rottner, M. Schaks, Assembling actin filaments for protrusion, Current Opinion in Cell Biology 56 (2019) 53–63, cell Architecture. doi:https://doi.org/10.1016/j.ceb.2018.09.004.
URL https://www.sciencedirect.com/science/article/pii/S0955067418301108

[3] E. S. Chhabra, H. N. Higgs, The many faces of actin: matching assembly factors with cellular structures, Nature Cell Biology 9 (10) (2007) 1110–1121. doi:10.1038/ncb1007-1110.
URL https://doi.org/10.1038/ncb1007-1110

[4] R. J. Petrie, K. M. Yamada, At the leading edge of three-dimensional cell migration, Journal of Cell Science 125 (24) (2012) 5917–5926. arXiv:https://journals.biologists.com/jcs/article-pdf/125/24/5917/2116743/jcs-125-24-5917.pdf, doi:10.1242/jcs.093732.
URL https://doi.org/10.1242/jcs.093732

[5] G. Jacquemet, I. Paatero, A. F. Carisey, A. Padzik, J. S. Orange, H. Hamidi, J. Ivaska, FiloQuant reveals increased filopodia density during breast cancer progression, Journal of Cell Biology 216 (10) (2017) 3387–3403. arXiv:https://rupress.org/jcb/article-pdf/216/10/3387/1066267/jcb_201704045.pdf, doi:10.1083/jcb.201704045.
URL https://doi.org/10.1083/jcb.201704045

[6] M. K. Driscoll, E. S. Welf, A. R. Jamieson, K. M. Dean, T. Isogai, R. Fiolka, G. Danuser, Robust and automated detection of subcellular morphological motifs in 3d microscopy images, Nature Methods 16 (10) (2019) 1037–1044. doi:10.1038/s41592-019-0539-z.
URL https://doi.org/10.1038/s41592-019-0539-z

[7] S. Nilufar, A. A. Morrow, J. M. Lee, T. J. Perkins, Filodetect: automatic detection of filopodia from fluorescence microscopy images, BMC Systems Biology 7 (1) (2013) 66. doi:10.1186/1752-0509-7-66.
URL https://doi.org/10.1186/1752-0509-7-66

[8] D. Tsygankov, C. G. Bilancia, E. A. Vitriol, K. M. Hahn, M. Peifer, T. C. Elston, CellGeo: A computational platform for the analysis of shape changes in cells with complex geometries, Journal of Cell Biology 204 (3) (2014) 443–460. arXiv:https://rupress.org/jcb/article-

pdf/204/3/443/1362993/jcb_201306067.pdf, doi:10.1083/jcb.201306067.
URL https://doi.org/10.1083/jcb.201306067

[9] D. J. Barry, C. H. Durkin, J. V. Abella, M. Way, Open source software for quantification of cell migration, protrusions, and fluorescence intensities, Journal of Cell Biology 209 (1) (2015) 163–180. arXiv:https://rupress.org/jcb/article-pdf/209/1/163/1368276/jcb_201501081.pdf, doi:10.1083/jcb.201501081.
URL https://doi.org/10.1083/jcb.201501081

[10] V. Urbančič, R. Butler, B. Richier, M. Peter, J. Mason, F. J. Livesey, C. E. Holt, J. L. Gallop, Filopodyan: An open-source pipeline for the analysis of filopodia, Journal of Cell Biology 216 (10) (2017) 3405–3422. arXiv:https://rupress.org/jcb/article-pdf/216/10/3405/1066410/jcb_201705113.pdf, doi:10.1083/jcb.201705113.
URL https://doi.org/10.1083/jcb.201705113

[11] C. Castilla, M. Maska, D. V. Sorokin, E. Meijering, C. Ortiz-de Solorzano, 3-d quantification of filopodia in motile cancer cells, IEEE Transactions on Medical Imaging 38 (3) (2019) 862–872. doi:10.1109/TMI.2018.2873842.

[12] S. I. Mousavi, K. M. Pearce, S. Scarlata, E. Tüzel, Re-track: Software to analyze the retraction and protrusion velocities of neurites, filopodia and other structures, Analytical Biochemistry 596 (2020) 113626. doi:https://doi.org/10.1016/j.ab.2020.113626.
URL https://www.sciencedirect.com/science/article/pii/S0003269719309194

[13] J. G. Lefevre, Y. W. H. Koh, A. A. Wall, N. D. Condon, J. L. Stow, N. A. Hamilton, Llama: a robust and scalable machine learning pipeline for analysis of large scale 4d microscopy data: analysis of cell ruffles and filopodia, BMC Bioinformatics 22 (1) (2021) 410. doi:10.1186/s12859-021-04324-z.
URL https://doi.org/10.1186/s12859-021-04324-z

[14] D. V. Sorokin, I. Peterlík, V. Ulman, D. Svoboda, T. Nečasová, K. Morgaenko, L. Eiselleová, L. Tesařová, M. Maška, Filogen: A model-based generator of synthetic 3-d time-lapse sequences of single motile cells

with growing and branching filopodia, IEEE Transactions on Medical Imaging 37 (12) (2018) 2630–2641. doi:10.1109/TMI.2018.2845884.

[15] M. M. Bagonis, L. Fusco, O. Pertz, G. Danuser, Automated profiling of growth cone heterogeneity defines relations between morphology and motility, Journal of Cell Biology 218 (1) (2018) 350–379. arXiv:https://rupress.org/jcb/article-pdf/218/1/350/1378868/jcb_201711023.pdf, doi:10.1083/jcb.201711023.
URL https://doi.org/10.1083/jcb.201711023

[16] C. B. Barber, D. P. Dobkin, H. Huhdanpaa, The quickhull algorithm for convex hulls, ACM Trans. Math. Softw. 22 (4) (1996) 469–483. doi:10.1145/235815.235821.
URL https://doi.org/10.1145/235815.235821

[17] H. Cevikalp, H. S. Yavuz, B. Triggs, Face recognition based on videos by using convex hulls, IEEE Transactions on Circuits and Systems for Video Technology 30 (12) (2020) 4481–4495. doi:10.1109/TCSVT.2019.2926165.

[18] X. Zhang, C. Wang, X. Fan, Convex hull-based distance metric learning for image classification, Computational and Applied Mathematics 40 (4) (2021) 113. doi:10.1007/s40314-021-01482-x.
URL https://doi.org/10.1007/s40314-021-01482-x

[19] R. Cupec, I. Vidović, D. Filko, P. Durović, Object recognition based on convex hull alignment, Pattern Recognition 102 (2020) 107199.
URL https://www.sciencedirect.com/science/article/pii/S0031320320300066

[20] Z. Guo, C. Liu, X. Zhang, J. Jiao, X. Ji, Q. Ye, Beyond bounding-box: Convex-hull feature adaptation for oriented and densely packed object detection, in: Proceedings of the IEEE/CVF Conference on Computer Vision and Pattern Recognition (CVPR), 2021, pp. 8792–8801.

[21] M. Maška, O. Daněk, S. Garasa, A. Rouzaut, A. Muñoz-Barrutia, C. Ortiz-de Solorzano, Segmentation and shape tracking of whole fluorescent cells based on the chan–vese model, IEEE Transactions on Medical Imaging 32 (6) (2013) 995–1006. doi:10.1109/TMI.2013.2243463.